Acta Astronautica, Volume 176, November 2020, pp. 139-155
DOI: 10.1016/j.actaastro.2020.06.003

Drop Your Thesis! 2018 results: 4.74 seconds of microgravity conditions to enable future cubesat landings on asteroids

Gautier F.[a*], Sitepu E.[b], Le Blay C.[c], Kersey G.[d], Sánchez J.P.[e*]

School of Aerospace, Transport and Manufacturing, Cranfield University, College Road, Cranfield, Bedfordshire, United Kingdom MK430AL, [a] florian.gautier.borrallo@gmail.com, [b] elioenai.sitepu@cranfield.ac.uk, [c]carole.leblay@gmail.com, [d] g.kersey32@gmail.com, [e] jp.sanchez@cranfield.ac.uk.
* Corresponding Author

Abstract

Space exploration has seen a growing number of asteroid missions being launched; mostly due to their scientific interest, but also on account of the potential impact threat and prospective valuable resources of their targets. Landing safely on the surface of an asteroid is one of the main technical challenges before obtaining in-situ observations and ground-truth data. Given the asteroid's extremely weak gravitational field, purely ballistic descent trajectories become a suitable option to reach its surface. However, this is still a very risky operation due to the limited knowledge of the object's physical characteristics. Hence, deploying a small lander is often a more conservative option than endangering the mothercraft itself, and thus a simple CubeSat may provide a low cost solution for asteroid exploration. However, for a CubeSat system to be able to safely land on the surface of an asteroid, a sufficient dissipation of energy must naturally occur at touchdown, or else the resultant bouncing may lead to high uncertainties on the final landing location, or even yield an escape trajectory. This paper describes the result of ESA Academy's Drop Your Thesis! 2018 (DYT2018) programme. DYT2018 carried out a microgravity experiment, led by Land3U team from the Astronautics and Space Engineering Course at Cranfield University, to provide additional data on the engineering constraints relevant to land a CubeSat on the surface of an asteroid. The experiment was performed in ZARM's Drop Tower, located in Bremen, during two Drop campaigns in November 2018 and February 2019. A total of 7 drops were completed, each providing 4.74 seconds of microgravity under vacuum environment. The experiment measured the coefficient of restitution of a 1U mock-up, equipped with a 4-kg mass, touching down on the simulated asteroid surface with an average velocity of 150 mm/s. Three successful drops measured a coefficient of restitution of 0.26±0.03.

Keywords: Coefficient of Restitution, CubeSat Landing, Asteroid, Microgravity, Drop Your Thesis, ZARM Drop Tower

Nomenclature

ϵ: Coefficient of restitution value
g_0: Earth surface standard gravity
GP1: GoPro camera n°1
GP2: GoPro camera n°2
FC: ZARM Fast Camera
v_{td}^{-}: Velocity before touchdown
v_{td}^{+}: Velocity after touchdown
σ: Standard deviation of the error

Acronyms/Abbreviations

Complementary Metal–Oxide–Semiconductor (CMOS)
Coefficient of Restitution (COR)
European Space Agency (ESA)
European Space Agency Exploration Sample Analogue Collection (ESA^2C)
High Efficiency Video Coding (HEVC)
Japan Aerospace Exploration Agency (JAXA)
Portable Network Graphics (PNG)
Release Mechanism (RM)
Region of Interest (ROI)
Zentrum für angewandte Raumfahrttechnologieund Mikrogravitation (ZARM)
Speeded Up Robust Features (SURF)
Computer Aided Design (CAD)

1. Introduction

Exploration of the Solar system requires knowledge of its earliest instances of its formation, of which asteroids are the primal remnants. While remote study of these celestial objects has been performed, missions are now more interested in using landers to explore its surface and interior.

Although the extremely weak gravitational field on these objects allows the possibility of landing [1], it remains a technical challenge, as demonstrated by the failed landing of MINERVA during Hayabusa (JAXA) [2] and Philae landers (ESA) [3]. The recent success of the Hayabusa2 (JAXA) landers such as MASCOT [4] showed the advantages of using smaller landers to lower the risk on the global mission. Following this perspective, CubeSats are considered one of the best options to undertake high risk secondary missions at low cost as the successful MarCO CubeSats from NASA InSight Mission demonstrated. ESA is also considering embarking a 6U CubeSat [5] for its HERA mission towards the binary asteroid system Didymos and Didymoon.

The landing phase is the most critical for asteroid exploration as the weak gravitational field also reduces the escape velocity. Therefore, any attempt at landing would aim to reduce the impact velocity and assure that enough energy is dissipated upon impact. The Land3U team, formed by 6 students from Cranfield University, United Kingdom, simulated the landing of a CubeSat on the surface of an asteroid. This experiment aimed at bridging the gap between low energy dissipation measured during the impact of Philae and Hayabusa [3, 6, 7] and high dissipation estimated from previous low-velocity experiments in microgravity [8-11].

This experiment was performed through the Drop Your Thesis programme, which enables students to have access to the ZARM Drop Tower in Bremen. This permits experiments to be performed in an environment with a very low level of microgravity, at 10^{-6} g_0, which enables the study of phenomena observed in space or on the surface of bodies with very low levels of gravity, such as asteroids. A CubeSat mock-up, equipped with a 4-kg mass, represented a future asteroid lander. It was released with a 150 mm/s velocity onto a simulated rocky asteroid surface. As previous studies used a spherical impactor [8-11], the Land3U team experimented instead with a cubic shape which is believed to better represent current trends for landers, and particularly future opportunities for interplanetary CubeSats. Five drops were initially planned to be performed in November 2018. Due to technical issues two supplementary drops were sponsored in February 2019. Therefore, a total of seven drops were performed, each providing 4.74 seconds of microgravity. Difficulties due to the microgravity environment were encountered and only the last three drops provided data to measure the velocities. These velocities allowed the computation of the coefficient of restitution (COR) as a means of measuring the energy dissipation. While not providing data on the rebound, the first drops demonstrated the difficulties on the use of regolith in an environment with a low level of microgravity.

This paper presents the results obtained from both of the experiment campaigns. The first section is dedicated to the experiment set-up and looks at some of the challenges of creating a representative asteroid environment on the Earth. Then, the experiment campaigns are discussed, followed by the analysis of the results, detailing the techniques that were performed and measurements that were undertaken to obtain values for the COR. Following this, the issues encountered during the campaigns and lessons learned from these issues are examined, which then leads into further discussion and future work. Finally, the conclusions from the experiment campaigns are summarized.

2. Experiment Set-up

The Land3U experiment was envisaged as an Earth based experiment whose results should help on the design of future landing operations for unpowered landers, i.e. those with no active control system. In particular, the experiment aimed to answer the following question; *how much energy dissipation may occur naturally during a ballistic landing touchdown of a 3- to 4-kg spacecraft?* The landing craft was chosen to be a small CubeSat, likely of 3U shape factor, and thus with a mass of 3 to 4 kg. The experiment focused on the measurement of the normal coefficient of restitution to characterize the energy dissipation during the experiment.

In order for the experiment to be successful and inform the architecture and design of future small body exploration missions, the environmental conditions needed to be as close as possible to those encountered on asteroids. In particular, the following three key environmental aspects were identified: the level of gravity had to be as close as possible to those encountered on such small astronomical bodies; the level of vacuum had to be as high as possible; and the touchdown surface needed to be as relevant as possible to those potentially encountered on the surface of asteroids.

The requirement with regard to the microgravity conditions led to the conclusion that, amongst all the ESA Academy's Gravity-related programmes[1], the most suitable conditions were offered by the ZARM Drop Tower at the University of Bremen, as indeed the microgravity achieved at ZARM is very close to those expected on asteroids. The need to perform the experiment in vacuum was initially a difficult problem to solve. However, upon consultation with the engineers at ZARM, it was also discovered that JAXA had used the very same drop tower when carrying out deployment test experiments for the Hayabusa2 landers. JAXA was contacted and generously agreed to let the Land3U team use the same vacuum chamber that they had purpose-built for their tests. Finally, the asteroid surface was initially created by using ESA 03-A KM Bentonite granules, a simulant lend by ESA Exploration Sample Analogue Collection (ESA2C). However, as discussed in Section 3, problems with the behavior of this material in the transition to microgravity led to some modifications being necessary.

The following key aspect of the experiment design was the landing/touchdown velocity, which needed to be within the range expected by an unpowered lander [1]. This was to be accomplished by the use of a release mechanism, consisting of a compressed spring and electromagnet. When microgravity conditions were achieved, an appropriate automatic trigger would cut the power on the electromagnet. In consequence, the stored mechanical energy in the spring would push down the CubeSat, propelling it towards the regolith surface at the required velocity.

[1] https://www.esa.int/Education/ESA_Academy

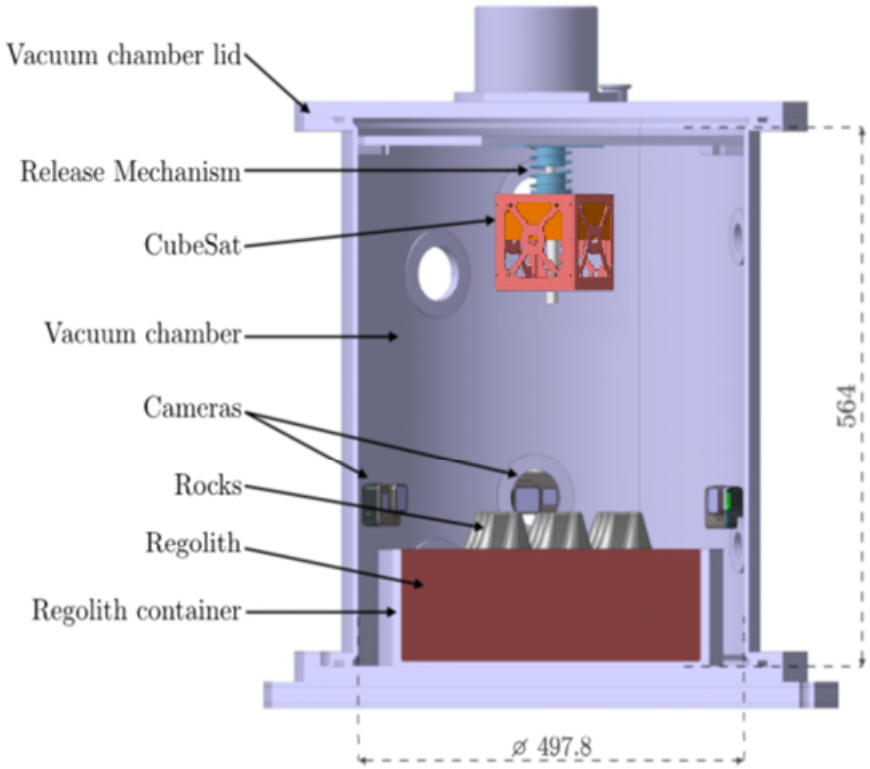

Figure 1 : Annotated cross section of experiment set up inside JAXA vacuum chamber with the internal dimensions of the vacuum chamber (in mm)

125

Figure 1 shows the experiment setup inside JAXA's vacuum chamber. Starting at the top of the vacuum chamber is the lid. Underneath this is the release mechanism, which is holding the CubeSat in place by use of an electromagnet. There is then a gap of about 240 mm between the base of the CubeSat and the top of the regolith surface (h in Figure 2). This gap is to ensure that the simulated touchdown occurs about 2 seconds after the capsule
130 is released, whilst the entire experiment is in microgravity, assuming a velocity of between 100 to 200 mm/s. A light gate was placed (orange in Figure 2) above the impact point, with an emitter and receptor diametrically opposed. Cameras were place to view the CubeSat side, focusing ~6 cm above impact point. The regolith was held in a container in order to allow for easy installation and removal between drops. This container was attached to the base of the vacuum chamber and had mounting points drilled in the walls of the container to allow for
135 positioning of high speed cameras for observation of the touchdown.

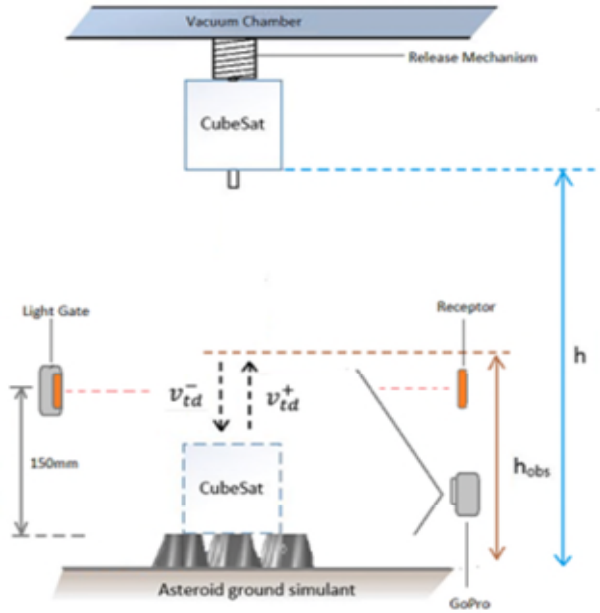

Figure 2: Schematic of experiment set-up. Release mechanism is fixed to the vacuum chamber structure and retain the CubeSat before the drop. CubeSat bottom side is separated by ~240mm from the impact zone (h). Camera field is focused on the estimated position of impacting CubeSat. Laser gate (orange) was placed above the rocks to ensure CubeSat passing through entirely.

2.1. ZARM Drop Tower and Operations.

Microgravity experiments on the Earth are usually performed using parabolic flights, rockets or drop towers. The ZARM Drop Tower in Bremen is one of the facilities of ZARM (Center of Applied Space Technology and Microgravity) [12]. The ZARM Drop Tower is ideally suited to simulate the microgravity environment encountered near small asteroids, because the quality of the microgravity conditions reached at ZARM is of order 10^{-6} g_0. Small asteroids have extremely weak gravitational environment, and these microgravity conditions are very similar to those experienced in the surface of visited asteroids, such as those of asteroid 25143 Itokawa.

Microgravity experiments are accommodated inside a specially designed drop capsule. The capsule is pressurized at atmospheric pressure and sealed from the vacuum of the outer drop tube of drop tower. The capsule is equipped with power source, sensors and connections for external control. The Land3U experiment was integrated inside the drop capsule provided by ZARM (see Figure 3).

Figure 3. (Left) Experiment setup inside JAXA's vacuum chamber, mounted inside open ZARM Capsule. (Centre) Land3U team. (Right) ZARM Capsule being winched up to the top of the tower.

Once the experiment was integrated inside the vacuum chamber, the high-speed cameras inside were started. The lid was then placed on and bolted down, and the high speed cameras on the outside of the capsule were positioned as required using the view from an external monitor to guide the alignment. The vacuum tubing was attached, along with a connection to a remotely operated valve that would be opened shortly before the drop to create the internal vacuum.

As soon as the ZARM team had carried out their checks, the whole assembly was then wheeled over to the inside of the drop tower. The lid and external cover of the capsule were attached, taking care to connect the Wi-Fi router (used for communication between the capsule and the control room) and attaching the vacuum hose to the lid. The capsule was then winched up to the top of the tower.

Once the capsule reached the top of the tower, the doors to the internal and external tubes were closed, and the interior tube was pumped down to around 10 Pa. This vacuum was necessary to avoid any drag affecting the capsule and thus the experiment inside. The pumping down to vacuum took about an hour, after which the Land3U team was ready to commence their experiment. The valve on the vacuum chamber was opened, which vented the air inside the chamber to the inside of the drop tower tube. The cameras on the inside and outside of the vacuum chamber were set to record, and once the capsule had been disconnected from the drop tower umbilical, the experiment began.

It takes 4.74 seconds for the capsule to traverse the distance from the top to the base of the tower. The Land3U experiment aimed to achieve a landing about two seconds after release, since the behaviour of the CubeSat in microgravity after impact could then be observed.

Before a drop, the capsule was held at the top of the tower and the CubeSat maintained in position by the release mechanism. At the beginning of the drop, the capsule was released and started falling down the inner tube of the tower. The CubeSat was held in position for the first 0.5 seconds of the drop – this was to allow any vibrations caused by the release of the capsule to dampen out, since these vibrations could have a negative effect on the experiment. Once this time had elapsed, the capsule control system activated the spring-based release mechanism, which ejected the CubeSat with a velocity of 150 mm/s. The CubeSat was guided for 40 mm by a central rod (within the release mechanism) before entering a 200 mm freefall. The impact on the simulated asteroid ground happened on average 1.6 s after release. The remaining seconds of microgravity were used to observe the behaviour of the rebound. At the end of the drop, the capsule and experiment suffered a deceleration force of between 25 g_0 and 50 g_0 due to the deceleration chamber at the base of the ZARM drop tower. The full drops were observed through cameras to determine the velocity of the CubeSat after rebound and estimate the COR. A timeline of the experiment is summarized in Figure 4.

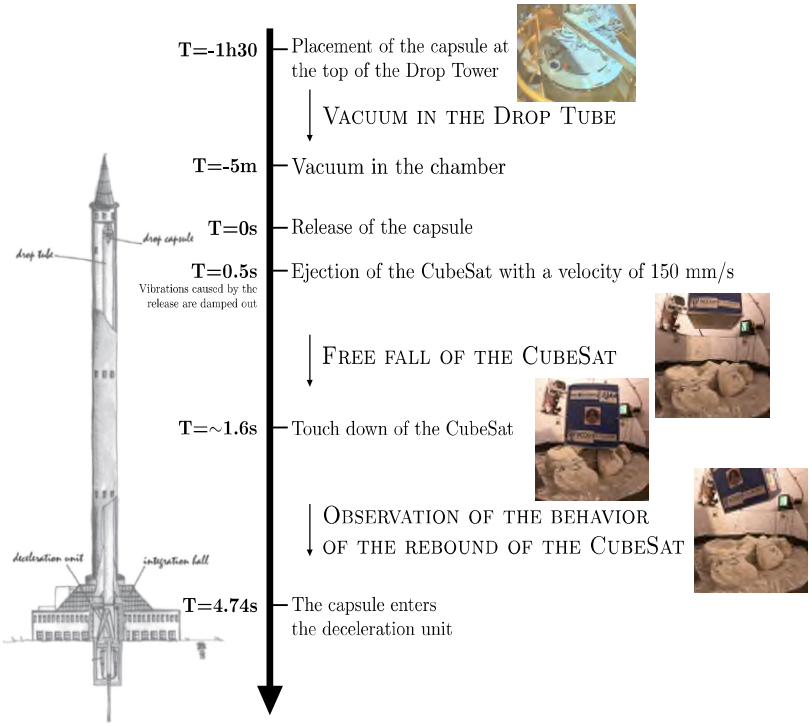

Figure 4. Experiment's timeline

2.2. *CubeSat & Release Mechanism*

Since the aim of the experiment is to inform future missions to asteroids, the landing element of the experiment needed to replicate a potential future lander. The CubeSat is a recently developed standard of nanosatellite that has proved its efficiency to perform high-risk missions at low price [13]. Use of CubeSats for realizing a perilous task such as landing on asteroids could be one of their future applications.

The first aim was to use a 3U CubeSat, a standard that has been considered for ESA's mission proposals [14]. However, due to the limited vertical space available in the vacuum chamber, a 3U-sized lander was not deemed feasible and a 1U volume was chosen instead. A 1U sized lander would ensure there was sufficient available experiment space for the rebound of the lander to proceed unhindered by walls or other parts of the experiment.

Following the fact that there is a clear correlation between the COR of a rebound and the inertial mass of the bouncing object, our 1U CubeSat mock-up was designed with a mass matching the total mass expected for a 3U CubeSat. Hence, our 1U CubeSat should be approximately 4 kg. The importance of this is also described in previous Earth COR determination experiments [15], and thus a 4 kg load was maintained in the Land3U experiment.

Another particular feature of our 1U CubeSat mock-up is the presence in the top and bottom face of a hole in the middle to allow for the rod used to guide the fall as part of the release mechanism. The purpose of the guiding rod is then to minimize the tilting of the CubeSat during that fall. The tilting issue was a consequence of the design of the release mechanism, and particularly of the interface between the upper part of the release mechanism and the CubeSat. The upper part was made of two magnets – one electromagnet at the top of the capsule and one magnet on the CubeSat – both surrounded by a spring that provided a velocity in the range of 100 – 200 mm/s at touchdown. Maintaining a consistent compression of the spring was important as the touchdown velocity per drop needed to be all within +-10 mm/s. Both a pendulum and an air-bearing table set-up were implemented and used to determine the required spring compression for the LAND3U experiment, as well as the expected consistency and accuracy of the resultant release velocity. The test results allowed to verify that the consistency of the released velocity was under the 10 mm/s threshold [16].The test also showed that the release mechanism yielded indeed a slight rotation to the CubeSat, most likely due to the spring failing to provide a completely uniform push. This effect was alleviated by the use of a guiding rod. To minimize friction between the CubeSat and the rod, a linear ball-bearing held in place by a shaft was put inside the CubeSat.

The release mechanism was controlled by ZARM's Capsule Control System (CCS) to ensure a consistent release between the drop. The CCS automatically released the CubeSat 500 ms after the initial capsule drop in order to allow sufficient time for the initial release vibrations on the capsule to damp out.

Figure 5 shows a schematic of both the CubeSat and the release mechanism as placed inside the vacuum chamber. Each color represents a part of each system: pink for the structure of the CubeSat, orange for the mass, blue for the magnets and spring of the release mechanism and white for the rod. In the cross-section view shows the linear ball-bearing inside the CubeSat. As the centre of the gravity needed to be as high as possible in order to yield an inertia matrix as close as possible to the one expected for a 3U landing system, the mass was cut in the middle to perfectly fit the shaft and still be the thinnest possible.

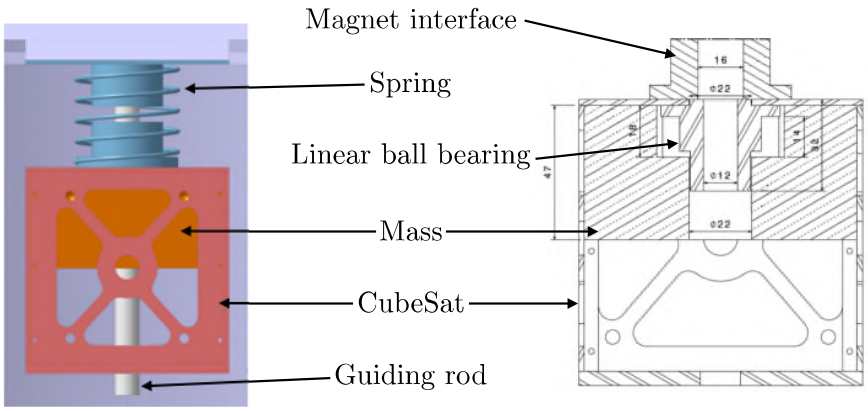

Figure 5. (Left) CubeSat and Release Mechanism as placed inside the vacuum chamber. (Right) Cross section of the CubeSat and the RM elements attached to it (magnet interface and linear ball bearing) (units in cm)

Table 1 summarizes the characteristics of the CubeSat and the Release Mechanism

Table 1. CubeSat and Release Mechanism properties

CubeSat properties	
Dimensions	100x100x100 mm
Mass	3.882 kg
Position of the centre of mass (origin at a bottom corner of the CubeSat)	50 mm 50 mm 71.7 mm
Release Mechanism properties	
Spring constant	290 N/m
Guiding rod	Length of 130 mm

2.3. *Sensors*

The main sensors to measure the velocity were high-speed cameras. A total of four high speed cameras were used in the experiment. Three were mounted at touchdown level to measure the velocity before the impact, while the fourth was positioned on top of the chamber.

Two high-speed cameras, as shown on the Figure 1, were fixed to the cylindrical container, spaced by a 90° angle to be in front of a different face of the CubeSat. These cameras were both "GoPro Hero6 Black" which were chosen for their small volume, their reliability and their capacity to record in 1080p resolution at 240 frames per seconds (fps). Due to lens restriction, the field of view was a wide one with some fish-eye distortion. Due to storage volume and heating in the low-pressure environment, those two cameras were remotely controlled through Wi-Fi to start recording just before the drops. For convenience, the GoPro camera on the left side is referred as GP1 while the GoPro on the right side is referred as GP2 (see Figure 6).

Two other high-speed cameras were provided by ZARM and relied on a Digital High-Speed CMOS Imaging System. Since they were not adapted to a low-pressure environment, they were placed out of the vacuum chamber but inside the ZARM capsule and they could observe the chamber interior using small windows in the vacuum chamber structure. However, due to placement constraint, only one of these cameras could record the rebound area by being placed on the external side of the chamber. This camera is later referred as FC and was placed at 45° from each GoPro. Although it provided a fast recording capacity (500 fps), the resolution of this camera was low (512x512 pixels).

A light gate was also added to have a further validation of the CubeSat's velocity before impact. An emitter and receptor were fixed on opposite sides of the chamber, at 110 mm above the impact point. When the CubeSat was released, it cut the laser beam and the change in signal level was seen by the receiver. By measuring the duration of this eclipse, the CubeSat velocity could be deduced.

In order to record the scene drop with high speed cameras, an important lightening was required in the closed vacuum. This was provided by external lamps attached to the chamber side. (see

Figure 6. Sensors Setup. The external view (left) shows the bottom FC camera and two lamps attached to windows on the side of the vacuum chamber. The interior view (right) shows the two GoPros, separated by 90°, with the FC camera seen from the middle window. The light gate is seen attached at the top of the container, with the receptor (right side in blue) diametrically opposed to the emitter.

Table 2 summarizes the sensors present during the experiment.

Table 2: Sensors review

Sensors Name	Type	Placement	Characteristics	Objectives
GP1	camera	Inside the Vacuum chamber	GoPro, 1080p resolution, 240fps	Record drop and rebound to measure velocity of CubeSat.
GP2	camera	Inside the vacuum chamber, 90° degrees	GoPro, 1080p resolution, 240fps	Record drop and rebound to measure velocity of CubeSat.
FC	camera	Outside the vacuum chamber, 45° from GPs	Digital High-Speed CMOS, 512x512 pixels, 500fps	Record drop and rebound to measure velocity of CubeSat.
Light Gate	laser	Fixed 15cm above impact zone		Measure velocity of CubeSat before rebound. Constantly monitoring from chamber closing.

2.4. *The Regolith Bed*

This section presents the method and production of setting up regolith analogue. There are two regolith analogue set-ups being used throughout the experiment. The initial set-up was inspired by the smooth zone of the Muses Sea on asteroid Itokawa which is composed of numerous, size-sorted granular materials ranging from several centimetres to sub-centimetres scales as shown in Figure 7 [6]. However, an issue was found during the first the experiment where the regolith bed started to float out of the contained at the instant the capsule was dropped. As a response to this issue, the team came up with another regolith analogue set-up, which simulated a rocky surface on an asteroid. Figure 10, which is a close-up image of the surface of asteroid Bennu was taken as an inspiration to produce this final set-up.

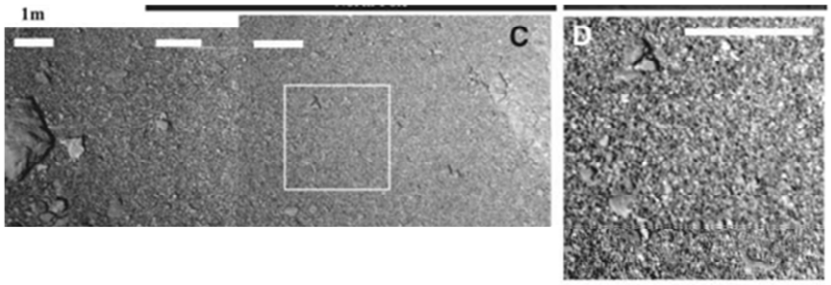

Figure 7. The Muses Sea). The rectangle in left image indicates the size of the image on the right. The scale bars on both images are 1 m [6].

Initial Regolith Analogue Set-up. Based on the available information prior to the release of images and scientific information from Hayabusa 2 and OSIRIS-Rex missions, the Land3U team decided to simulate a fine granular regolith inspired on the smooth zone (i.e. The Muses Sea) at the surface of asteroid Itokawa (see Figure 7). The particular rationale followed for this was that a ballistic landing would likely target (if possible) such a smooth landing zone in order to minimize the risk of damaging the lander. This fine granular surface was replicated by utilizing ESA03-A KM Bentonite granules, a simulant from ESA^{2}C that can reasonably represent chemical, mineralogical, mechanical and physical characteristics of the wider C-type asteroids, as well as Phobos and Deimos. One of the main reasons this simulant was selected was the similarity of its mechanical and physical properties; in addition, the ease of acquiring this material was an essential consideration. The material was stored in Natural History Museum in London, UK and loaned out for free to Land3U team.

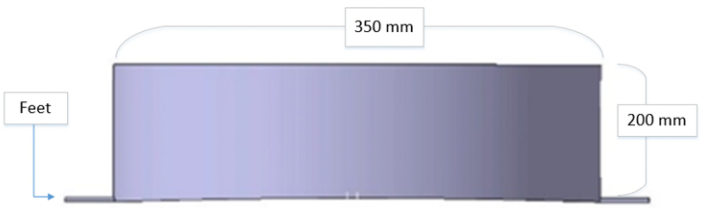

Figure 8. CAD representation of a slightly curved container base

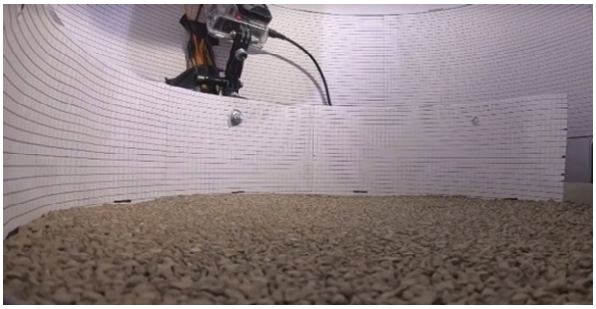

Figure 9: Surface analogue initial set-up. Regolith bed of simulant ESA03A – KM Bentonite

The initial simulant set-up consisted of pouring the ESA03-A KM Bentonite granules into a container, followed by mixing, compressing and ensuring a touchdown surface as flat as possible. The container was a cylindrical 2 mm thick aluminium plate with a height of 200 mm and a diameter of 350 mm. It had 4 feet on the base which could easily be bolted onto the experiment platform (vacuum chamber). However, due to its manufacturing process, the base of the container was slightly curved as seen in Figure 8. Figure 9 shows the final results of this process. As can be seen in Table 3, the resultant mechanical properties of the initial simulant set-up were indeed similar to those of known and relevant asteroids, such as 101955 Bennu.

Table 3. Comparison of initial set-up to Bennu mechanical properties

	101955 Bennu	Initial Set-up
Grain density	2000 - 2900 kg/m^3 [17]	2440 kg/m^3
Bulk density	1190 ±13 kg/m^3 (OSIRIS-REx value) [18]	1050 kg/m^3
Macro Porosity	50 - 60% [19, 20]	56%
Average particle size	<1cm (Pre-encounter value) - TBD for OSIRIS-REx value [18]	2.24 mm
Particle size range	0.5 - 4.0 cm [17]	53 µm - 4.75 mm
Granular bed thickness	0.8 to 3.0 cm (Diurnal skin depth)[17]	8.5 cm

Final Regolith Analogue Set-up. However, as soon as the experimental campaign began, problems with the stability of the initial granular set-up became evident and a new asteroid surface simulant had to be designed. The problem occurred during the transition from 1 g_0 to 0 g_0 (i.e. release of the capsule at the top of the drop tower), which triggered, likely due to the vibrations induced by the release, a motion to the granules of the simulant. Hence, a new configuration that would be able to fix the granules to the container was necessary. This issue is presented in section 3.1, as well as in Section 5.1, which presents some post-experiment analysis to further understand it.

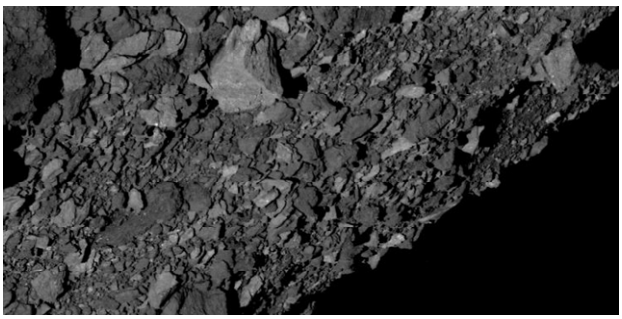

Figure 10. Image of Bennu's rocky surface. The large, light-colored boulder just above the center of the image is about 24 feet (7.4 meters) wide, which is roughly half the width of a basketball court [21].

At the time, the recently released images of Ryugu's and Bennu's surfaces, as seen in Figure 10, inspired the final set-up of the asteroid surface simulant. These images showed a surface featuring ubiquitous small stones [21]. Given the apparent lack of smooth zones in these latter asteroids, Land3U attempted to mimic this rocky surface conditions by adding marble rocks on top of the simulant bed.

Finally, to keep the regolith in place, plastic film (2-3 thin layers) was used to wrap the simulant. The films were set to be slightly loose to avoid increasing the compactness of the regolith layer. The marble rocks were then placed on top on the simulant bed, also held by meshed wires attached firmly at the side of the container, as seen in Figure 11. This layer of rocks thus served two purposes; helping to fix the wrapped regolith onto the container and preventing the CubeSat from interacting with the plastic/elastic texture of the film used to wrap the regolith. The set of rocks were placed directly underneath the CubeSat trajectory, with the wired mesh holding the rocks in such a way that direct contact of the CubeSat to marble rocks was ensured, rather than the CubeSat interacting with the wires. This configuration prevented rocks from moving up while minimally affecting the impact phase. To sum up, this final surface analogue set-up had two types of layers; a simulant bed of ESA03A – KM Bentonite and a series of marble rocks.

Figure 11. Surface analogue Final Set-up. Addition of rocks on top of ESA03A – KM Bentonite

3. Experimental Campaign

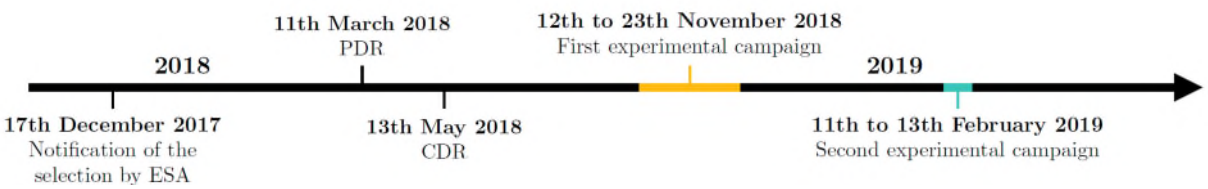

Figure 12. Campaign's timeline

The project started in January 2018 after notification of selection by ESA, as seen in Figure 12 and went through several design milestones during the following months. One of the challenges was to design the entire experiment

to fit inside JAXA's vacuum chamber having access only to the CAD file of the vacuum chamber. Following the experimental design, each part was built and shipped to ZARM to be available for the integration week.

The experimental campaign initially took place over 2 weeks from the 12th to 23rd November 2018, including a first week of integration and a second week with one drop per day for a total of five drops. The issues described in the following section led to having three more days of experimental campaign from 11th to13th February 2019 with one day to set up the experiment and two more drops on the following two days.

The integration week was split between the accommodation of our experiment's main parts to JAXA's vacuum chamber, which had not been accessible up to that point, and the testing of sensors and release mechanism in the vacuum environment. This week led to some slight modifications being made in the attachment points and structures to improve robustness.

During the second week, the issue with the simulant (see Section 2.4) placed a heavy focus on design modifications and replacement for the simulant. This is further detailed in Section 3.1. A significant wind velocity on the second day prevented the tower from carrying out any drop, so the team had to prepare for carrying out two drops in one day. This happened on the fourth day of this second week. The drops and issues faced are examined in more detail in this section following sections details the drops and issues faced during the drops. A brief summary of all of the drops can be found in Table 4.

Table 4: Summary of campaigns drops.

Drop #	Date	Change from previous configuration	Observations & Issues
Drop 1	19/11/2018	-	Upward movement of regolith. CubeSat going through the cloud of regolith
Drop 2	21/11/2018	Stratification of regolith with aluminum foils	Faster upward movement of regolith. CubeSat going through the cloud of regolith.
Drop 3	22/11/2018	Replacement of simulant	Upward movement contained. No regolith escaping. CubeSat stopped on the rod.
Drop 4	22/11/2018	Change for spare ball bearing unit and guiding rod	Rebound observed. One GoPro lost. Issue in recording system of ZARM high speed camera. Only 1 set of data from remaining GoPro. Laser not working.
Drop 5	23/11/2018	-	Rebound observed. Issue in recording system of ZARM high speed camera. Only 2 set of data from remaining GoPros and laser measurements.
Drop 6	12/02/2019	-	Rebound observed. Slower velocity observed at release. All set of data acquired.
Drop 7	13/02/2019	Adjustment of spring compression	Rebound observed. Velocity compensated. All set of data acquired.

3.1. *Early issues in the experimental setup*

A major issue of the early experiment set-up was found out at Drop 1: the regolith bed showed an undesired movement during the drop. A solution to this issue had to be found in both a very short period of time (i.e., 24 to 48h) and at a negligible cost (due to budget constraints). This section explains the issues and modifications made until Land3U produced a usable asteroid surface analogue. A minor issue also occurred because of the release mechanism.

Regolith bed issue. The initial regolith set-up showed undesired behavior when it was dropped. As soon as the capsule was released, hence it transited from 1 g_0 to 10^{-6} g_0, the regolith simulant started moving slowly upwards. The motion of the regolith top layer appeared fairly homogenous, with the top layer moving at about 25 mm/s. As a consequence, the regolith compactness had decreased significantly after the 1 second it took the lander to reach the top layer, with the result that the lander simply sank into the regolith, and thus no coefficient of restitution could be measured (i.e. no rebound). Figure 13, shows the phenomena in Drop 1. The two images show the state of the regolith bed before and 1 seconds after the drop.

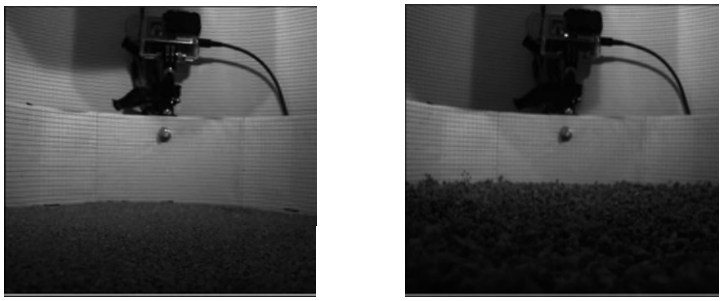

Figure 13. (left) Simulant initial position. (Right) Simulant position after 1 seconds at Drop 1.

At the following day, for Drop 2, the team was still aiming on solely using the regolith simulant without any significant intervention. The first attempt to eliminate this floating regolith behavior was to add multiple thin layers of aluminum foil and plastic film in between the regolith. The approach was an attempt to dampen the upwards movement. For this, multiple double-layers of plastic film and aluminum foil were placed within the regolith from bottom to top, with a spacing of 10 mm between them (regolith bed has a thickness of 50 mm). The top layer featured a 50 mm diameter circular hole on the middle, such that the lander could interact directly with the regolith bed. However, as Figure 14 demonstrates, the modification was ineffective at damping the motion, but increased instead the velocity of the regolith traversing the upper circular hole of foil to 67 mm/s. Therefore, this approach was abandoned.

Initially Land3U were only given 5 drops. However, with only three drops available left, the urgency of solving this matter became highly crucial. Land3U intended to have a minimum three identical experiments, as it was necessary to produce a statistically robust result. This meant that the next asteroid surface analogue set-up (for Drop 3) had to be used for the following drops (Drop 4 and Drop 5).

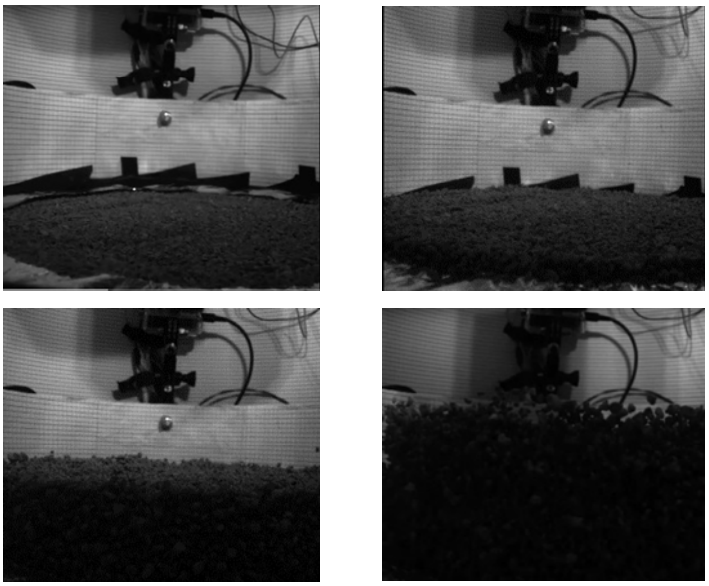

Figure 14. The state of regolith bed in Drop 2 at several time step. (Left-top) Simulant initial position, (Right-top) Simulant position at 0.3s. (Left-bottom) simulant at 0.6s. (Right-bottom) simulant at 1s.

For the following and final regolith configuration several modifications were implemented. First of all, the container was modified. The base of the container was not completely flat, as shown in Figure 8, but instead was slightly curved due to the way in which it had been manufactured. By adding the mass of the simulant (8.5 kg), the base was forced flat. A possible explanation for the behavior of the regolith was that the bottom part of the container (i.e. 2 mm thick aluminum plate) relaxed back to its original curvature, transferring some linear momentum to the regolith. Therefore, to avoid any vibration induced by the base of the container during the transition to 10^{-6} g_0, the base was removed, so that the simulant would sit directly over the base of the experiment

platform (JAXA vacuum chamber). As shown in Figure 15, the base of the chamber is thicker (~30 mm) and was predicted not to have a significant relaxation which could potentially eliminate the issue.

Still, there was no mechanism to firmly attach the simulant bed to the base and if this issue was merely because of the simulant bed or granular interaction properties, then this floating phenomenon would persist in Drop 3. Given the urgency to solve the issue, Land3U opted to add further modifications to ensure the regolith would be firmly hold to the container. Hence, the *final regolith analogue set-up*, as described in Section 2.4, was devised and implemented in order to de-risk the remaining Drops.

Figure 15. The experiment platform (Vacuum chamber from JAXA)

The wrapping of the regolith and the fixing of the marble rocks on the *final regolith analogue set-up* was ensured to be sufficiently loose so that no artificial compactness was added, but sufficiently firm that the vibrations observed in Drop 1 and 2 would not disassemble the set-up. As can be observed in Figure 16, despite plastic film wrapping and wires fixing, some upward movement of the set-up can still be observed during the initial moments of the subsequent drops, although this movement is now quickly damped by the wires holding the final set-up. The damping period lasted for 0.4 seconds before it reached its relaxed position for CubeSat impact. As shown in Figure 16, there was a gap between the red and yellow line, which compares the initial position (red) and 0.09 seconds after (yellow) the release of the rock at the center front. This was the maximum gap observed before it was pulled to its initial position. The wires kept this configuration steady and therefore, this final set-up was kept for the rest of the drops.

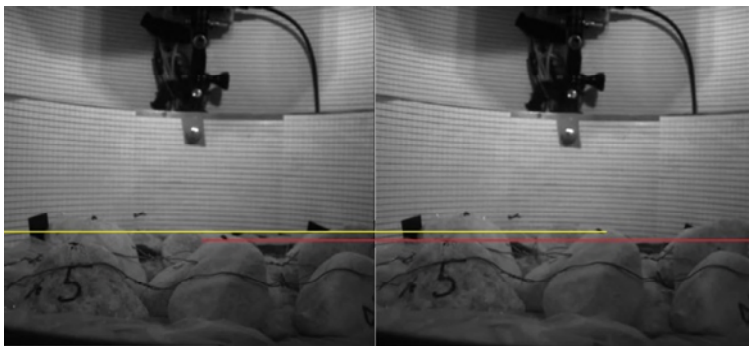

Figure 16. Images of Simulant surface before (left) and 0.09 second after released (right).

Once the modifications to the simulant were made, the third drop occurred and as planned, the simulant stayed in place. However, this drop was not successful either, as the CubeSat did not fall from the release mechanism. At the beginning of the drop, the CubeSat was indeed released from the electromagnet, but it did not slide to the end of the rod. It is believed that it was caused due to the friction between the rod and the CubeSat. Before each drop, the sliding was tested and indeed, it showed a slight increase of resistance between each drop. However due to a restrictive number of changes due to limited spares, the third drop required the use of the same pair of rod and ball bearing unit as for the initial two drops.

3.2. *Successful drops*

During the first campaign, five drops were performed, from which the team managed to produce two completely successful experiments. This is: the CubeSat was released and a landing and rebound could be observed whilst in microgravity, on the screen in the control room at ZARM. However, for both of these drops, the high-speed cameras that had been provided by ZARM did not manage to record the successful drops. An overheating of the GoPros on the fourth drop and the malfunction of the laser sensor lead to only the fifth drop to have enough data collected to perform the estimations of velocities.

In order to get more reliable data and result, it was agreed between ESA and ZARM that the Land3U team would be allowed to carry out two more drops during a much shorter second experimental campaign in February 2019. Both of these later drops were successful. As a result, Land3U managed to perform three successful repeats of the experiment which was adequate to produce a reliable source of data, although only two video recordings of the drop and rebound were available. Those three successful experiments are studied in section 4 to estimate the coefficient of restitution

4. Measured Coefficient of Restitution

Following the work of Celik and Sanchez [1], the intended touchdown velocity was generally aimed at about 180 mm/s. However, due to lack of calibration of the release mechanism and the substantial re-setting necessary between the Drop 5 and the Drops 6 and 7, the final achieved velocity features some variability. Due to resources and timing constraints, the Drops 6 and 7 were performed by two team members, of which only one was present during the first campaign. This resulted in slight differences in positioning of the spring. Indeed, the velocity, while aimed at 180 mm/s, was observed to be lower than previous drops. In addition, a possible reason for this difference was the wear and tear of the guiding rod and the ball bearing unit. While a slightly higher friction was observed when testing the rod, the lack of additional spare parts prevented any replacement and might have caused the velocity difference observed during the drop. Also, while the Drop 5 yielded a relatively flat touchdown on the bed of rocks, and a relatively straight bounce with little rotation, the Drops 6 and 7 featured a higher rotational speed of the CubeSat after the touchdown, probably suggesting a spring push that was not perfectly vertical.

4.1. *COR Definition*

The Coefficient of Restitution (COR) is a tool used in impact studies to allow a simple modelling of the complex transfers of energy. The COR is hardly obtainable by any other means than experimentation and is influenced by many parameters that characterize both the objects impacting and the surface (or other object) being impacted. Our approach to determine it is based on Asteriou and Tsiambaos (2018) [20] and MASCOT papers on the landing

simulations [15, 22], where explanations on the different explicit COR definitions available in the literature can be found.

The simplest representation of the COR is to define a ratio based on the velocity before and after the impact. By splitting this velocity into normal and tangential components to the surface of impact, the following COR components can be identified:

$$COR_n = \frac{v_{td_n}^+}{v_{td_n}^-}$$

$$COR_t = \frac{v_{td_t}^+}{v_{td_t}^-}$$

The above definition does not take into account rotation as relevant for our approach as only the vertical velocity after the impact is to be studied. Thus, hereafter COR will refer to this definition of a velocity defined coefficient of restitution and only on the normal coefficient (i.e. COR_n).

Figure 17. CubeSat entering the field of view of the camera. This picture was obtained through extraction of the 6th drop videos recorded by the GoPro camera.

4.2. Data analysis

Drops #5, #6 and #7 were analysed separately for each camera available (two GoPros and 1 fast camera). The full recordings were split manually into the phases of landing and rebound (i.e. before and after the touchdown). From the analysis point of view, these phases are defined by the range of exploitable frames. The landing phase starts when the CubeSat enters the field of view of the camera (Figure 17) and stops when the CubeSat contacts the rocks. The rebound phase starts when the CubeSat loses contact with the bed of rocks and stops when the capsule hits the bottom of the tower or when the targeted face cannot be identified due to large rotation (Figure 18).

The objective of the analysis is to provide the estimated values of the velocity before and after the touchdown for each camera and for each drop.

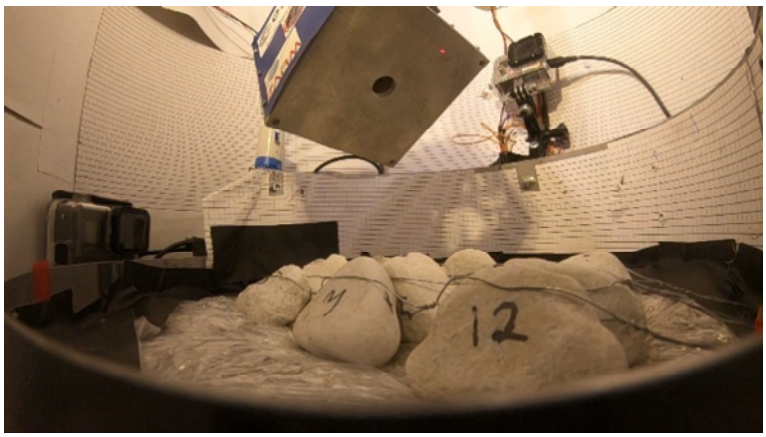

Figure 18. Large rotation of the CubeSat due to impact on the rock surface. This picture was obtained through extraction of the 7th drop videos recorded by the GoPro camera before any processing.

4.2.1 Video processing and feature tracking

Videos obtained from the GoPros were in MP4 format in the H.265 coding format (compressed format). All the processing on the videos was performed using MATLAB software and its open libraries.

The method applied relies on the analysis of the recorded video frame by frame. By splitting and uncompressing, data was produced in the Portable Network Graphics (PNG) format. PNG images are encoded in RGB and have 1920x1080 pixels resolution allowing high precision support for image processing.

The optics inside the GoPro cameras deforms the video through Fish Eye effect. This effect distorts the border of the image and this distortion affects the features on the CubeSat. In order to be able to calibrate the frames, and obtain the relation between pixels and real world distance, this effect had to be taken into account. The process of calibration was performed using the checkerboard method. This consisted of recording a chessboard with known dimensions to obtain the intrinsic and extrinsic parameters of the camera [23]. This also allows undistorting the frames thus getting rid of the Fish Eye effect. Using the same checkerboard method, a plane of observation is defined where all pixels are associated to real world points using the focal length of the camera and the known characteristics of the checkerboard (squares area). This plane is the same as the observed face of the CubeSat front of the camera. It provides extrinsic parameters to define camera orientation and positioning to the observed scene. These parameters are then used to obtain the transformation from pixels to mm. This pre-process is also part of the referred calibration.

After the pre-processing actions, the actual tracking of the CubeSat can be performed. The tracking in each frame relied on the detection of features unique to each face of the CubeSat. First, a region of interest was created using a colour thresholding method [24] to shorten the tracking process. This colour segmentation masked the uninteresting region of the picture and needed to be robust to the brightness changes happening during the drop caused by the CubeSat motion. This constraint led to the use of the HSV colour space rather than RGB, an encoding of colours that better handles the change of light levels.

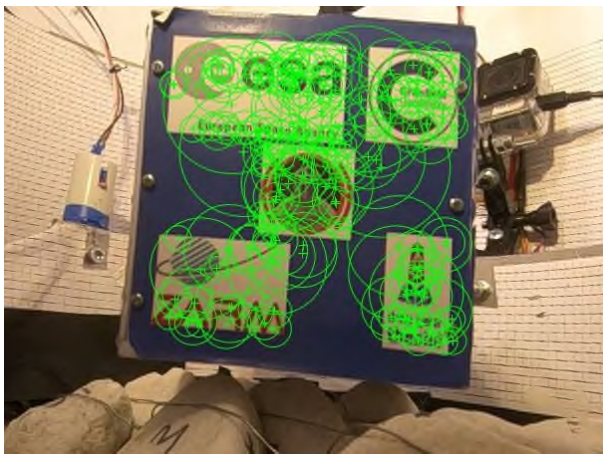

Figure 19. Cropped undistorted frame showing the features detected and tracked on the CubeSat surface.

This region of interest was then scanned to find features using the Speeded Up Robust Features (SURF) method [25]. Detecting a feature relies on the feature descriptors, which gather smaller interest points (Gaussian derivative, moments invariant…) in the neighbourhood to create an identifiable feature. The faster and more robust the descriptor is, the better the detection. The SURF descriptor focuses on assigning a circular region of interest around a feature and assigning an orientation (see Figure 19). This method is already implemented in MATLAB as the 'detectSURFFeatures' function.

A filtering was then performed to restrict those features to the strongest ones; subsequently a matching process was performed between two consecutive pictures [26] based on those features. Matched features were obtained which were then filtered using a RANSAC method to differentiate inliers and outliers [27] (see Figure 20). The selected features (i.e. matched) are all considered with the same weight in the velocity analysis.

Figure 20. Cropped montage of consecutive frames with the strongest matched feature.

Using the previous calibration of the cameras, the pixels' coordinates can be changed to real world position in order to measure displacement of the CubeSat in the vertical plane of the drop. This displacement was computed for each pair of matched features and averaged for the whole CubeSat from this, and knowing the framerate of the video recording, a velocity could then be estimated for every frame. A least square method is then performed to estimate the constant vertical velocity of the CubeSat before and after the impact. Note that the assumption of constant velocity before and after the touchdown is accurate given the quality of the microgravity conditions achieved in the ZARM drop tower.

Figure 21 and Figure 22 show the velocity estimation for the drop #5 before and after the rebound. During the contact between the rocks and the CubeSat, the velocity variation is not tracked. All velocity estimations and the

standard deviations for those values are gathered in Table 5. The time 0 is arbitrarily defined to the beginning of each phase analysed. Finally, by computing the ratio of the velocity after the rebound to velocity before it, the coefficient of restitution (COR) could be determined for each successful drop.

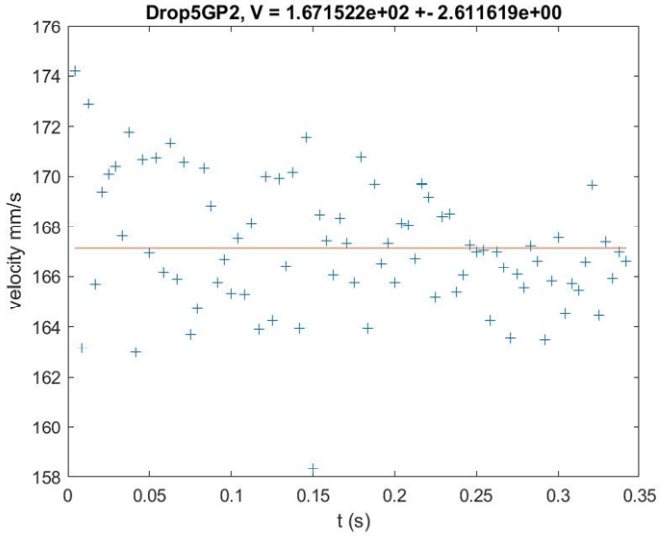

Figure 21. Measurements and estimation of CubeSat's velocity during the landing phase. The red line shows the least square estimated velocity. Time 0 is the start of the landing phase, when the CubeSat front face enter the field of view of the camera.

Due to small misplacements due to the computational detection and selection of the different features between two consecutives frame, inherent errors in CubeSat position are created giving this *noisy* distribution around the estimated value. On the landing phase (Figure 21), the velocity distribution of the matched features seems to be settling with time. This can be associated to the CubeSat moving from the rear of camera's field of view to its centre; i.e., moving from a more distorted to a minimal distortion region. While it is more apparent on some of the cameras, small velocity variation are also be the result of calibration errors affecting the position estimation of the CubeSat.

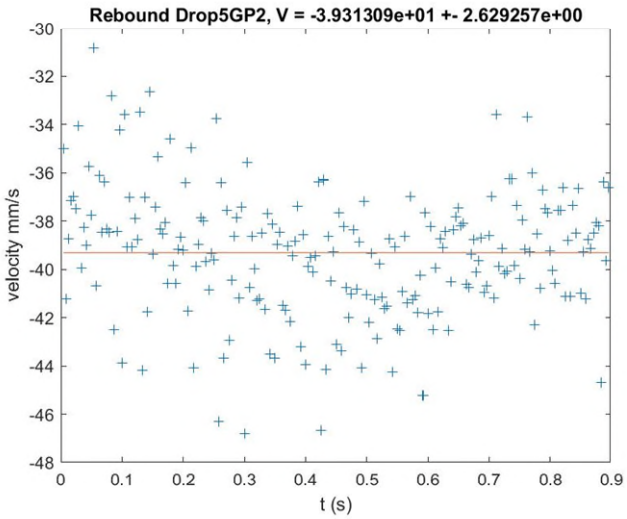

Figure 22. Measurements and estimation of CubeSat's velocity after the rebound. The red line shows the least square estimated velocity.

Table 5: Estimated velocities by least square method for each camera and associated standard deviation.

	Camera	Initial Velocity (mm/s)	σ (mm/s)	Rebound Velocity (mms/s)	σ (mm/s)
Drop 5	GP1	168.5	4.2	37.3	2.8
	GP2	167.2	2.6	39.3	2.6
Drop 6	GP1	147.8	4.3	40.7	2.8
	GP2	148.2	3.3	38.3	3.7
	FC	149.0	4.6	42.9	4.5
Drop 7	GP1	164.5	2.5	43.8	2.3
	GP2	163.6	3.3	33.8	2.6
	FC	160.5	6.2	48.9	7.1

Another visualization of the results showed in Table 5 is found in the graph of Figure 23. The FC camera's higher standard deviation is explained by a lower resolution compared to the GoPro which induces more error in the tracking of features.

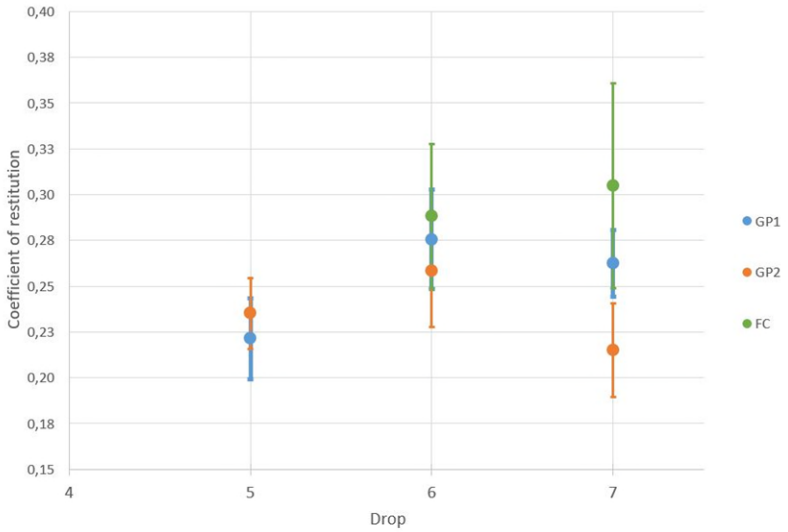

Figure 23. Estimated coefficient of restitution for each drop and each camera.

4.2.2 *Laser gate measurements*

In parallel, laser gate detectors were also used to validate the method described above for optical estimation of the vertical velocity. The laser receptor produced a varying signal depending on the intensity of light received. Through analysis of this signal, the duration of eclipse due to the CubeSat shadowing the receptor could be measured. As the CubeSat rotation was negligible during the pre-touchdown phase, the CubeSat's vertical velocity could be estimated, from the eclipse duration. However, after the rebounds, the CubeSat rotation was not negligible anymore and prevented a similar estimation from being carried out (see Figure 24). Indeed, the shape of the CubeSat shadow that was cast on the receptor was different because of this rotation.

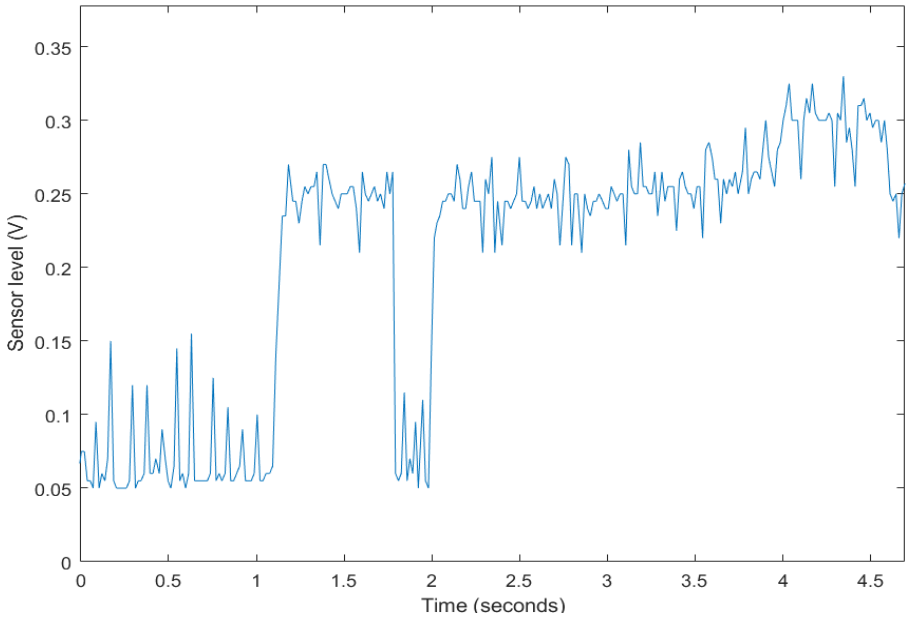

Figure 24. Sampled laser signal of Drop 7. The plot represents the luminosity level measured by the laser receptor over time. The lower signal level (0.05 V) is associated with ambient light level (laser + lamps). The higher level (0.25 V) is a marker of the laser being eclipsed by the CubeSat. The eclipse lasted for less than a second, then the rebound happened and another eclipse occurred, lasting until the end of the drop.

The velocities estimated through the laser measurements only required knowledge of the CubeSat dimensions to convert eclipse time to velocity. Those estimations allowed a validity check on the accuracy of the velocities measured by image processing of the videos recorded by the cameras. Thus, the velocities before the impact were validated by the laser's velocity measurements. Those values are available in Table 6.

Table 6: Velocity measurement before the impact by laser.

	Initial Velocity (mm/s)	Uncertainty (mm/s)
Drop 5	170.5	4.9
Drop 6	148.8	4.2
Drop 7	161.2	4.6

These velocities can be compared to the one showed in Table 5 from the cameras. The difference is less than 5 mm/s, which supports the concordance between the two types of sensors.

4.3. *COR estimates and accuracies obtained*

The knowledge of these velocities allows the computation of the estimated coefficients of restitutions which are shown in Table 7.

Table 7: Estimated coefficient of restitution for each measurement and drops and its associated error.

	Camera	Estimated COR	Error
Drop 5	GP1	0.22	0.022
	GP2	0.24	0.019
Drop 6	GP1	0.28	0.027
	GP2	0.26	0.031
	FC	0.29	0.039
Drop 7	GP1	0.26	0.018
	GP2	0.22	0.026
	FC	0.30	0.056

The error on each coefficient of restitution is here taken as the worst-case linear sum of errors in the velocity components for the decent and rebound measurements:

$$\Delta\varepsilon = \left|\frac{1}{v_{td}^{-}}\right| . \sigma_{v_{td}^{+}} + \left|\frac{v_{td}^{+}}{v_{td}^{-\,2}}\right| . \sigma_{v_{td}^{-}}$$

The error on the COR depends on both error on the velocity before touchdown ($\sigma_{v_{td}^{-}}$) and error the velocity after touchdown ($\sigma_{v_{td}^{+}}$).

Those errors are written in Table 7. A higher error can be seen for the ZARM fast camera. This increased error is mainly due to the lower frames resolution for this camera. By computing the average value for each drop, we obtained the values in Table 8:

Table 8: Averaged COR values for each drop and associated errors

	Initial Velocity	Estimated COR	Error
Drop 5	171mm/s	0.23	0.021
Drop 6	149mm/s	0.27	0.032
Drop 7	161mm/s	0.29	0.033

5. Issues and Lessons Learned

Land3U performed a total of 7 experiments. There were unsuccessful and successful experiments. However, many lessons were learned also from the unsuccessful drops at the beginning of the campaign. This section attempts to understand the causes of these unsuccessful drops and provide a potential solution to overcome those issues.

5.1. *Lessons learned from regolith bed issues*

The upwards movement of the regolith bed kept occurring during the drops. Our initial hypothesis is that the floating regolith problem may be caused by the natural elastic expansion of the regolith bed, rather than solely caused by external forces, such as transit vibrations of the structure of the vacuum chamber or the regolith container. If so, the behaviour would persist regardless of the smoothness of the transition from 1 g_0 to 10^{-6} g_0.

This section attempts to gain some insight into the expected expansion of the regolith simulant during the 1 g_0 to 10^{-6} g_0 by re-creating drop #1 in a computer simulation of LAMMPS (Large-scale Atomic/Molecular Massively Parallel Simulator) [28]. These are the parameters being considered by the simulation; grain elasticity (Young Modulus), density, coefficient of friction between particles, coefficient of restitution between particles and porosity. The simulation used a value of 2440 kg/m^3 for grain density, 0.52 for coefficient of friction (taken from the ESA^{2}C data base for ESA03A-KM Bentonite), assuming a coefficient of restitution of 0.2 and grain size distribution of 1.4 mm to 3 mm (in diameter) uniformly spread. Also, the individual grains were assumed to be fully spherical in the simulation.

There were three major steps in the simulation: insertion of regolith, relaxation (rest) of the regolith, and dropping the regolith in a free fall, as shown in Figure 25. All the simulations are compared to the actual regolith bed expansion in Drop 1, which is an expansion of about 35% after 1 second into the drop, with a starting 46% compactness. The simulation aims to study the relation between the grain elasticity and regolith bed expansion. The elasticity of the simulant (ESA03A-KM Bentonite) is unknown. Thus, the simulations used a variety of potential values; these were 0.1 MPa, 1 MPa, 10 MPa, 30 MPa, 50 MPa and 80 MPa. However, as a comparison, typical values of loose sand modulus Young ranges between 10 MPa to 30 MPa [29]. These six simulations with the above mentioned elasticity values created similar compactness (fill factor) of the initial regolith, at about 62%, which is more compact than that of the real regolith bed used.

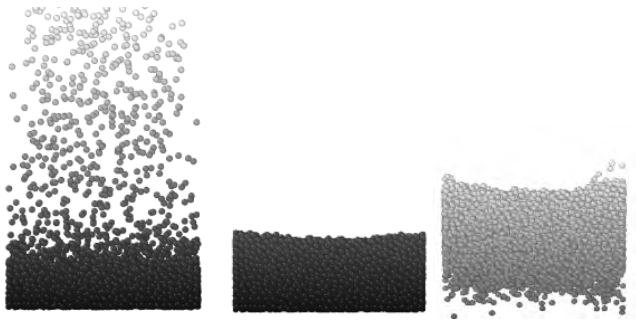

Figure 25. Three steps of the simulation. (Left) insertion of regolith, (Middle) regolith relaxation, (Right) regolith drop.

The expansions were then measured by comparing the standard deviations of the relative positions of each individual particle with respect to the barycentre of the ensemble of particles. Hence, the standard deviation of the initial ensemble σ_i (before the drop) is compared with the standard deviation of the ensemble after a 1 second drop simulation σ_f, and the ration σ_f/σ_i is then computed to represent the expansion of the simulated regolith bed. Figure 26 displays the relationship between expansion and grain elasticity of the computed results. It shows a decreasing expansion for an increasing grain elasticity value. Figure 26 shows both the initial ensemble of particles and the final ones for each simulated grain elasticity. The blue line represents the barycentre position, while the yellow lines represent the initial regolith thickness before the drop.

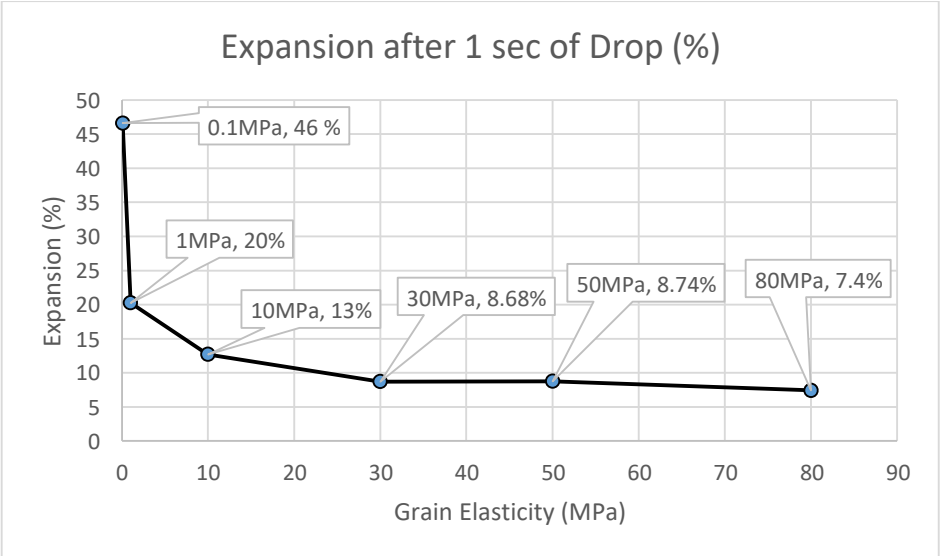

Figure 26. Relation of grain elasticity (E) to expansion of regolith bed after 1 second of drop.

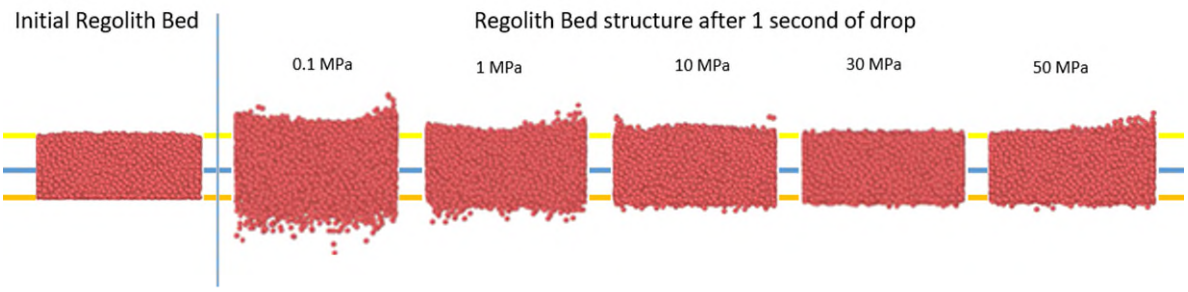

Figure 27. Images of granular expansion on various grain elasticity refer to its initial position (left). If referring to Gaussian Distribution approach, Blue line is the barycentre/mean and yellow lines are the initial regolith thickness.

The simulation results show lower expansion for the expected range of grain elasticity (10 to 30 MPa) than the actual phenomena in Drop 1, which was 35% expansion with 47% compactness in 1 second (non-spherical grains). Hence, this result are likely indicators that the behaviour is largely caused by the rapid transition to microgravity and natural expansion of the regolith bed. Given that the expansion measured in Drop 1 is nearly three times that expected according the results of the LAMMPS simulations, it seems to indicate that external vibrations from the structure of the vacuum chamber and drop capsule are likely contributors to the phenomenon. Nevertheless, the results also demonstrate that some floating behaviour should always be expected.

5.2. *Lesson learned from release mechanism issues*

The release mechanism design performed well for our experiment. Indeed, throughout all the drops, it provided a relatively constant and precise velocity to the CubeSat, allowing us to have consistent drops. Finally, as this experiment was a student-led, the low cost of this release mechanism was a definitive advantage.

However, the issue occurring at the third drop preventing the CubeSat from sliding along the rod showed us the limit of the system. As this problem never happened during our tests prior to the experiment week, we had to rapidly analyse all the parts and find a solution for the remaining drops. The easiest solution used was to test before each drop the rod and ball bearing and change the parts if the resistance was deemed high.

6. Further discussion

Focusing on the low velocity touchdown of a CubeSat on the surface of an asteroid, the coefficient of restitution estimated for a rocky surface (above relatively loose regolith) configuration can be found on Figure 23. The limited trials and the failures resulted in only three valid estimations of the coefficient of restitution.

According to our experiments then, an estimated range for COR during touchdown on a rocky surface (above relatively loose regolith) can be predicted to be between 0.2 and 0.35 considering an impact velocity ~150 mm/s. This range is lower than previous data collected from the missions Hayabusa and Rosetta. The first touchdown of the Hayabusa spacecraft measured a COR of 0.84 [6] but the uncertainty on this value is important due to the unknowns about spacecraft landing gears involvement. Philae, which was a 100 kg lander with a landing system specifically designed to minimize COR, seemed to measure a much lower COR value [3]. However, later analysis also provides higher estimates for the normal direction COR [7]. The work of Asteriou and Tsiambaos [20] showed how sensitive the coefficient of restitution is to landing conditions and the impactor properties such as mass and speed. On the other hand, previous experiments of small velocities in microgravity [8-11] did not observe rebound for regolith impacts at velocities lower than 200 mm/s. Those experiments were performed in fine regolith which, given the recent Hayabusa2 mission, show limitation on modelling asteroids to estimate coefficient of restitution. The results presented in this article are closer to the values found in recent JAXA experiment on hard surface impact [30]. Those experiments show the importance of knowledge of the surface properties to improve the landing capability.

Due to the non-flat impact created by a rocky layer, the CubeSat is subjected to a relatively large rotational state after the rebound. This rotation is difficult to predict due to the influence of the point of impact localization on rock edges and on the bottom surface of the CubeSat. Drops #5, #6 and #7 do show a variety of rotational states after rebound, while the corresponding CORs appear not to be hugely influenced by this.

The relevance of our COR measurements for an actual landing on an asteroid has to be investigated further. At this stage, the pressure distribution from the impact of the CubeSat mock-up to the regolith set-up is not yet studied. Once investigated, we can understand either the rebound is affected merely from the marbles or also from the ESA03-A KM Bentonite asteroid simulant.

7. Future work

The regolith expansion phenomenon was observed in all of the drops. However, there is a potential way to hold the regolith bed in place. At ZARM Drop Tower, 0.5 s is required after the start of the drop to fully enter microgravity phase. By this period, the floating has already occurred and by adding a cover on top of the regolith bed, it may prevent the upwards movement and keep the regolith in place. Then, when the experiment platform has entered microgravity phase, the cover can be retracted/opened. During the experiment campaign, Land3U did

not have the chance to test this technique due to limited amount of preparation time. This technique may be able to be used at other microgravity facilities, such as parabolic flight.

By reproducing the experiment, more data could be acquired and it could validate the reproducibility of our results. While the coefficient of restitution was the primary focus of this experiment, the data collected through the video media could allow reconstruction of the CubeSat both linear and angular momentums. This analysis could help understanding the energy transfer between the vertical acceleration and the rotating momentum.

Finally, placing sensors in the CubeSat to understand the modifications happening inside the regolith during the impact could provide more data for future asteroid seismologic studies. This is also the concept of the JUVENTAS CubeSat [5] on the HERA mission of the European Space Agency targeting the binary asteroids Didymos and Didymoon.

8. Conclusions

The Land3U team developed and performed in a microgravity experiment in drop tower to simulate the landing of CubeSats on the surface of asteroids. This paper described the results obtained and lessons learned from this experiment.

A total of 7 drops were performed in the ZARM Drop Tower, sponsored by ESA/ESA Academy, during two campaigns in November 2018 and February 2019. Only 3 drops allowed the retrieval of usable video data to estimate the coefficient of restitution. Nevertheless, all 7 drops led to interesting analysis and insights either on the experiment itself or on the unexpected phenomena with regards the asteroid surface simulant.

The coefficient of restitution estimated by our experiment shows a higher level of absorption than in previously reported data from past asteroids missions. Obviously, due to differences on the landing systems and conditions, it is difficult to explain the reasons for these differences. A potential explanation may be the elasticity and/or fluffiness of the surface material. Our Drop 1 experienced no bounce at all due to an increase on the fluffiness of the simulant, caused by the increase in volume of the simulant during the transition from $1g_0$ to $10^{-6}g_0$. Instead, Drops 5, 6 and 7 measured a coefficient of restitution of 0.26±0.03. This is still much lower than those measured in by past landers in small bodies (i.e. Philae and Hayabusa). A potential explanation may be that our asteroid surface simulant (marble rocks on top of a dry bed of porous granular material) is still substantially more elastic than that found in the likely hardened surfaces encountered by Philae and Hayabusa.

Acknowledgements

The authors of this manuscript would like to thank the Land3U team members Stuart Ogborne, Daniyal Durrani and Jonathan Prete for their valuable contributions to the design and implementation of the experiments here described. Similarly, we would like to thank Dr Jenny Kingston and Dr Luca Zanotti for their expert advice during the design phases of the Land3U experiments.

Land3U thanks also Nigel Savage; ZARM Team, Thorben Könemann, Jan Siemer and Fred Oetken; and ELGRA mentors, Dr. Philip Carvil and Álvaro Romero Calvo for the guidance during the preparation of this experiment. Also JAXA to allow us using one of their vacuum chamber, Cranfield University, Koel Berry, and. Dr Dayl Martin from ESA2C that provides insights during the selection of asteroid material analogue. Our sincere gratitude is also given to Mr Warley Rocha and Professor Kazuya Yoshida from Tohoku University, for their guidance and time in order to fully realize and perform the air bearing table experiment.

This work was sponsored by the Drop Your Thesis! 2018 programme. Access to the ZARM Drop Tower was granted through ESA/ESA Academy. The ESA03-A KM Bentonite was loaned from ESA2C, at no charge.

References

[1] O. Celik, J.P. Sánchez, Opportunities for Ballistic Soft Landing in Binary Asteroids, Journal of Guidance, Control, and Dynamics, 40 (2017) 1390-1402.

[2] J. Kawaguchi, A. Fujiwara, T. Uesugi, Hayabusa-Its technology and science accomplishment summary and Hayabusa-2, Acta Astronautica, 62 (2008) 639-647.

[3] J. Biele, S. Ulamec, M. Maibaum, R. Roll, L. Witte, et al., The landing(s) of Philae and inferences about comet surface mechanical properties, Science, 349 (2015).

[4] Y. Tsuda, T. Saiki, F. Terui, S. Nakazawa, M. Yoshikawa, et al., Hayabusa2 mission status: Landing, roving and cratering on asteroid Ryugu, Acta Astronautica, 171 (2020) 42-54.

[5] H. Goldberg, Ö. Karatekin, B. Ritter, A. Herique, P. Tortora, et al., The Juventas CubeSat in Support of ESA's Hera Mission to the Asteroid Didymos, in: Small Satellite Conference, Logan, Utah, 2019.
[6] H. Yano, T. Kubota, H. Miyamoto, T. Okada, D. Scheeres, et al., Touchdown of the Hayabusa spacecraft at the Muses Sea on Itokawa, Science, 312 (2006) 1350-1353.
[7] R. Garmier, T. Ceolin, T. Martin, A. Blazquez, E. Canalias, et al., Philae Landing on Comet Churyumov-Gerasimenko: Understanding of Its Descent Trajectory, Attitude, Rebound and Final Landing Site, in: International Symposium on Space Flight Dynamics (ISSFD), Munich, Germany, 2015.
[8] J.E. Colwell, M. Taylor, Low-Velocity Microgravity Impact Experiments into Simulated Regolith, Icarus, 138 (1999) 241-248.
[9] J.E. Colwell, Low velocity impacts into dust: results from the COLLIDE-2 microgravity experiment, Icarus, 164 (2003) 188-196.
[10] L.M. Seward, J. Colwell, M. Mellon, B. Stemm, Low-Energy Impacts onto Lunar Regolith Simulant, in: AAS/Division for Planetary Sciences Meeting Abstracts #44, 2012, pp. 311.308.
[11] N. Murdoch, I. Avila Martinez, C. Sunday, E. Zenou, O. Cherrier, et al., An experimental study of low-velocity impacts into granular material in reduced gravity, Monthly Notices of the Royal Astronomical Society, 468 (2017) 1259-1272.
[12] ZARM drop tower Bremen User manual, in, ZARM FABmbH, 2012.
[13] D. Selva, D. Krejci, Preliminary Assessment of Performance and Cost of a Cubesat Component of the Earth Science Decadal Survey, in: 27th Annual AIAA/USU Conference on Small Satellites, Logan, UT, 2013.
[14] R. Walker, D. Binns, I. Carnelli, M. Kueppers, A. Galvez, CubeSat Opportunity Payload Intersatellite Network Sensors (COPINS) on the ESA Asteroid Impact Mission (AIM), in: 5th Interplanetary CubeSat Workshop (iCubeSat), Oxford, UK, 2016.
[15] C. Maurel, P. Michel, J. Biele, R.-L. Ballouz, F. Thuillet, Numerical simulations of the contact between the lander MASCOT and a regolith-covered surface, Advances in Space Research, 62 (2018) 2099-2124.
[16] S. Ogborne, LAND3U Drop Your Thesis! 2018: Release Mechanism, in: School of Aerospace, Cranfield University, Cranfield, 2018.
[17] D.N. DellaGiustina, J.P. Emery, D.R. Golish, B. Rozitis, C.A. Bennett, et al., Properties of rubble-pile asteroid (101955) Bennu from OSIRIS-REx imaging and thermal analysis, Nature Astronomy, 3 (2019) 341-351.
[18] D.S. Lauretta, D.N. DellaGiustina, C.A. Bennett, D.R. Golish, K.J. Becker, et al., The unexpected surface of asteroid (101955) Bennu, Nature, 568 (2019) 55-60.
[19] M. Hamm, M. Grott, E. Kührt, I. Pelivan, J. Knollenberg, A method to derive surface thermophysical properties of asteroid (162173) Ryugu (1999JU3) from in-situ surface brightness temperature measurements, Planetary and Space Science, 159 (2018) 1-10.
[20] P. Asteriou, G. Tsiambaos, Effect of impact velocity, block mass and hardness on the coefficients of restitution for rockfall analysis, International Journal of Rock Mechanics and Mining Sciences, 106 (2018) 41-50.
[21] NASA(2019). Bennu Images Reveal Unexpected Discoveries. Available at: https://www.nasa.gov/image-feature/goddard/2019/bennu-images-reveal-unexpected-discoveries [Accessed 25 April 2020].
[22] F. Thuillet, P. Michel, C. Maurel, R.-L. Ballouz, Y. Zhang, et al., Numerical modeling of lander interaction with a low-gravity asteroid regolith surface, A&A, 615 (2018) A41.
[23] D. Scaramuzza, A. Martinelli, R. Siegwart, A Toolbox for Easily Calibrating Omnidirectional Cameras, in: 2006 IEEE/RSJ International Conference on Intelligent Robots and Systems, 2006, pp. 5695-5701.
[24] S. Sural, G. Qian, S. Pramanik, Segmentation and histogram generation using the HSV color space for image retrieval, in: Proceedings. International Conference on Image Processing, IEEE, 2002, pp. II-II.
[25] H. Bay, T. Tuytelaars, L. Van Gool, SURF: Speeded Up Robust Features, in, Springer Berlin Heidelberg, Berlin, Heidelberg, 2006, pp. 404-417.
[26] M. Muja, D.G. Lowe, Fast approximate nearest neighbors with automatic algorithm configuration, VISAPP (1), 2 (2009) 2.
[27] P.H.S. Torr, A. Zisserman, MLESAC: A New Robust Estimator with Application to Estimating Image Geometry, Computer Vision and Image Understanding, 78 (2000) 138-156.
[28] S. Plimpton, Fast Parallel Algorithms for Short-Range Molecular Dynamics, Journal of Computational Physics, 117 (1995) 1-19.
[29] Á. Kézdi, L. Rétháti, Handbook of soil mechanics, Elsevier Amsterdam, 1974.
[30] S. Wal, O. Çelik, K. Yoshikawa, Y. Tsuda, Y. Kawakatsu, Experimental Validation of Hard-Surface Impacts using Air-Bearing Assembly for Small-Body Landers, in: 32nd International Symposium on Space Technology and Science (ISTS 2019), Fukui, Japan, 2019.